Lennard-Jones Fluid Mixtures in Contact with Semipermeable Membranes. A Density Functional Approach

Paweł Bryk*,† and Stefan Sokołowski†

Department for the Modeling of Physico-Chemical Processes, Faculty of Chemistry, MCS University, 200-31 Lublin, Poland

Orest Pizio‡

Instituto de Química de la UNAM Coyoacán 04510, México D.F.

Received: April 28, 1998; In Final Form: November 30, 1998

A density functional approach based on Kierlik−Rosinberg theory is applied to a two-component Lennard-Jones mixture in contact with a selectively permeable membrane. The results of theoretical calculations are compared with the grand canonical ensemble Monte Carlo simulations. The density profiles obtained for temperatures higher than the critical temperature agree well with simulation data if the difference in the diameters of particles of two components is small. We have also obtained that the agreement between the theory and simulations is reasonable if the particles of the component that penetrates the membrane are twice larger than the particles of nonpenetrating component. For other diameter ratios and for the case when the density of the mixture is high, the theory disagrees with simulations. At temperatures lower than the critical temperature the theoretical density profiles also have been evaluated, and a possibility of multiple solutions of the density profile equation, corresponding to the existence of different phases, is discussed.

1. Introduction

The structure and thermodynamic properties of nonuniform simple fluids have been studied both by computer simulation and various theories, see, for example, refs 1 and 2. Among different theoretical approaches, the density functional theory has been proved to be one of the most successful in describing the structure and thermodynamics of nonuniform fluids.[3] In particular, the density functional theories, which include a weighted density approximation, have provided important insights into the layering and wetting transitions, and into other phase transformations near surfaces and in pores. However, commonly used *model* density functionals do not reproduce accurately the equation of state of a Lennard-Jones fluid, for example. The absolute values for the critical temperature and critical density predicted by the theory do not agree well with simulations.[4] The nonuniformity in a fluid can be caused by the presence of either impenetrable walls or of the walls being permeable to some (or all) species of the fluid mixture.[5−7] The investigation of the structure and thermodynamics of fluids near semipermeable surfaces, i.e., membranes, is of great importance for better understanding of the behavior of many physicochemical and biochemical systems. On the other hand these studies are also of interest in the construction of the theory of osmotic phenomena. A theory of partitioning of fluids through semipermeable membranes, based on an extension of the Ornstein−Zernike (OZ) integral equation for homogeneous fluids (or so-called first order, or singlet level equation), has been developed by Zhou and Stell.[8,9] The density profiles and osmotic pressure for fluids in contact with spherical and planar membranes have been obtained. Recently, Bryk et al.,[10] have applied an inhomogeneous Ornstein−Zernike (or the second order, or pair level) integral equation to investigate a hard-sphere mixture near a semipermeable surface. It was shown that the pair level approach for this model agrees better with Monte Carlo simulation data than the singlet level theory, but large memory allocation is required to solve the second-order equations. An alternative, simpler approach for the study of fluids in contact with semipermeable membranes can be based on the density functional theory. In our previous work,[11] we have applied a density functional method, based on the Kierlik−Rosinberg[12] formalism, to a binary mixture of hard spheres in contact with a planar semipermeable membrane. A reasonable agreement of the theory with simulation data has been obtained. The main objective of the present study is to extend the aforementioned density functional method for the case of model fluids with Lennard-Jones (LJ) interactions near selectively permeable membranes. Our primary goal in this work is to test the validity of the theory under different conditions.

Moreover, we will discuss the behavior of the subcritical fluid mixture near selectively permeable membrane. More generally, the phase behavior of fluid mixtures in contact with selectively permeable membranes is expected to be quite complex.

2. Theory and Simulation Procedure

Let us consider a two-component fluid mixture consisting of species A and B. The particles interact via the truncated LJ (12−6) potential,

$$u_{ij}^{\mathrm{LJ}}(r) = \begin{cases} 4\epsilon_{ij}\left[\left(\frac{\sigma_{ij}}{r}\right)^{12} - \left(\frac{\sigma_{ij}}{r}\right)^{6}\right], & r < r^{\mathrm{cut}} \\ 0, & \text{otherwise} \end{cases} \quad (1)$$

where i,j = A, B; ϵ_{ij}, σ_{ij} denote the LJ parameters and r^{cut} is the cutoff distance. The fluid is considered to be in contact with a semipermeable membrane, located in the plane $z = 0$. The

† Email: (stefan. pawel)@hebe.umcs.lublin.pl.
‡ Email: pizio@servidor.unam.mx.

10.1021/jp982028r CCC: $18.00
Published on Web 04/14/1999

membrane is assumed to be impermeable for species A but totally permeable for particles belonging to species B. As in earlier studies,[8−11] the membrane is considered as a source of an external field that creates inhomogeneity of the system. The interaction potential between the membrane and species A is chosen as

$$v_A(z) = \begin{cases} 0 & z < 0 \\ \infty & z > 0 \end{cases} \tag{2}$$

However, we assume that the particles of species B do not interact with the membrane, such that $v_B = 0$ in the entire system. Our theoretical development for the system in question is based on the Kierlik−Rosinberg approach of the density functional theory,[12] which has been derived from an earlier work by Rosenfeld.[13] Similar to any other density functional method,[2,3] this theory provides an approximation for the grand potential Ω as a functional of the fluid number densities $\rho_i(\mathbf{r})$, i = A, B

$$\Omega = F + \sum_{i=A,B} \int \rho_i(\mathbf{r})[v_i(z) - \mu_i]d\mathbf{r} \tag{3}$$

where μ_i is the chemical potential of species i. The Helmholtz free energy F is represented as a sum of an ideal and the excess terms: $F = \sum_{i=A,B} F_i^{id} + F^{ex}$. The ideal contributions are known exactly,

$$F_i^{id}/kT = \int \rho_i(\mathbf{r})[\ln(\lambda^{3/2}\rho_i(\mathbf{r})) - 1]d\mathbf{r} \tag{4}$$

where λ is the thermal wavelength. According to refs 2, 3, and 12, the excess free energy F^{ex} is divided into the reference hard sphere and the attractive parts, namely, $F^{ex} = F^{ex,hs} + F^{ex,att}$. The excess hard-sphere free energy is written down by using the Kierlik−Rosinberg functional,[12]

$$F^{ex,hs}[\rho_A,\rho_B] = \int \Phi(n_\alpha(\mathbf{r}))d\mathbf{r} \tag{5}$$

where Φ is the free energy density of a uniform hard sphere mixture. The excess free energy density follows from the Percus−Yevick compressibility equation

$$\Phi = -n_0 \ln(1 - n_3) + \frac{n_1 n_2}{1 - n_3} + \frac{n_2^3}{24\pi(1 - n_3)^2} \tag{6}$$

where n_α, $\alpha = 0, 1, 2, 3$, are the weighted densities,

$$n_\alpha(\mathbf{r}) = \sum_{i=1}^{2} \int \rho_i(\mathbf{r}')\omega_i^\alpha(|\mathbf{r} - \mathbf{r}'|)d\mathbf{r}' \tag{7}$$

and ω_i^α are the weight functions,

$$\omega_i^3(r) = \Theta(R_i - r)$$

$$\omega_i^2(r) = \delta(R_i - r)$$

$$\omega_i^1(r) = (1/8\pi)\delta'(R_i - r)$$

$$\omega_i^0(r) = -(1/8\pi)\delta''(R_i - r) + \delta'(R_i - r)/(2\pi r) \tag{8}$$

In eq 8, Θ denotes a step function, δ, δ', and δ'' are the delta function and its first and second derivatives, respectively, and R_i is the hard-sphere radius. The attractive force contribution to the free energy functional is considered in the mean-field approximation

$$F^{ex,att} = \frac{1}{2}\sum_{i,j=A,B} \int\int \rho_i(\mathbf{r})\rho_j(\mathbf{r}')u_{ij}^{att}(|\mathbf{r} - \mathbf{r}'|)d\mathbf{r}d\mathbf{r}' \tag{9}$$

The attractive part of the pair interaction between the fluid species $u_{ij}^{att}(r)$ is determined by using the Weeks−Chandler−Andersen[14] procedure,

$$u_{ij}^{att}(r) = \begin{cases} -\epsilon_{ij} & r < \sigma_{ij}^{min} \\ u_{ij}^{LJ}(r) & r > \sigma_{ij}^{min} \end{cases} \tag{10}$$

where $\sigma_{ij}^{min} = 2^{1/6}\sigma_{ij}$. The corresponding hard-sphere diameters, $d_{AA} = 2R_A$ and $d_{BB} = 2R_B$, can be evaluated from the Barker−Henderson approximation:[15]

$$d_{ii} = \int_0^{\sigma_{ii}^{min}} \{1 - \exp[-\beta(u_{ii}(r) - u_{ii}^{att}(r))]\}dr \tag{11}$$

where $\beta = 1/kT$. The density profile of both species have been obtained by minimization of the grand potential,

$$\delta\Omega/\delta\rho_i(\mathbf{r}) = 0 \qquad \text{for} \qquad i = A, B \tag{12}$$

Theoretical predictions have been tested versus grand canonical ensemble Monte Carlo simulations. The simulations have been carried out as follows. The parallelepiped unit simulation box with dimensions l_x, l_y, and l_z, has two semipermeable surfaces (membranes) embedded in the box. These membranes, located at $z = -l_z/2$ and at $z = 0$ are parallel to the XY plane. The periodic boundary conditions have been applied in all directions. The membrane located at $z = -l_z/2$ has thus its replica at $z = l_z/2$. The semipermeable membranes divide the cell into two subparts. In the region $-l_z/2 < z < 0$, particles of two species are present, whereas the region $0 < z < l_z/2$ is available only for B species. The cell elongation l_z must be large enough to ensure the existence of "bulk" parts in both subsystems. Following our earlier experience[16,17] we have used $l_x = l_y = 10$ and $l_z = 40$. Each Monte Carlo step has consisted of four trials: a trial to displace a particle, an attempt to create a particle, an attempt to delete a particle, and an attempt to change the identity of a particle (or to change the species flag).[18] The probability of a move is accepted according to the standard Metropolis scheme. The probability of acceptance of the creation step is[18]

$$P_{cr} = \min\left\{1, \frac{V_i\alpha_i}{N_i + 1}\exp[-\beta E_c]\right\} \tag{13}$$

whereas the probability of the acceptance of the annihilation step is

$$P_{del} = \min\left\{1, \frac{N_i}{\alpha_i V_i}\exp[-\beta E_c]\right\} \tag{14}$$

In the above, $\alpha_i = \exp(\beta\Delta\mu_i)$ is the activity of the component i, $\Delta\mu_i$ is the configurational (apart from kinetic contributions) part of the chemical potential of the component i, N_i is the number of particles of species i, E_c is the change of energy in a given step, $V_A = l_x l_y l_z/2$, and $V_B = l_x l_y l_z$. We recall that A particles can be present only in the left-hand side subpart of the system, consequently the volume V_i is different for different species. The swap step $i \rightarrow j$ is accepted with the probability[18]

$$P_{sw} = \min\left\{1, \frac{N_i\alpha_j}{(N_j + 1)\alpha_i}\exp[-\beta E_c]\right\} \tag{15}$$

It is evident that the creation of A particles can occur only if $z < 0$, and a swap step B $\rightarrow$ A is accepted only if the initial position of the B particle is between $-l_z/2$ and 0. The simulations have been carried out assuming equal probability of each trial step. The equilibration was established running the program for over 3×10^7 steps, and the ensemble averages were accumulated during 10^8 steps.

3. Results and Discussion

Our primary goals include computer simulation data for the model in question and is to test the density functional theory. We begin with the model for a simple set of parameters. Namely, we have assumed that both components of the fluid mixture are identical, $\epsilon_{AA} = \epsilon_{BB} = \epsilon_{AB} = \epsilon$. First, we would like to perform a comparison of the theoretical density profiles with the results of simulations. A comparison has been performed at a high temperature, $T^* = kT/\epsilon = 2$ and for three size ratios of the particles: $\sigma_{AA} = \sigma_{BB} = 1$ (the system I), $2\sigma_{AA} = \sigma_{BB}$, $\sigma_{AA} = 1$ (the system II) and $\sigma_{AA} = 2\sigma_{BB}$, $\sigma_{BB} = 1$ (the system III). In each case the size of smaller particles is taken as the unit of length. We have assumed that the cutoff distance r^{cut} is equal to $2.5\sigma_{BB}$, for the systems I and II, and $2.5\sigma_{AA}$, for the system III. Both components A and B mix ideally and the temperature $T^* = 2$ is higher than the critical temperature of one-component and of two-component system of LJ particles.

To compare the theory with simulations, we have applied the following strategy.[11] First, Monte Carlo simulations were performed. Next, from simulated profiles the left-hand side bulk densities (i.e., the densities in the two-component subpart of the system), ρ_{Al} and ρ_{Bl}, were evaluated. These densities have been used as an input in the density functional calculations. The density functional calculations can be also carried out using the chemical potentials as an input. Our methodology of comparison is justified by the fact that the computer simulations and the theory lead to different dependence of the chemical potential on the bulk density. Consequently, using the chemical potentials as an input to the density functional calculations, we would get other bulk densities on both sides of the membrane. The method of calculations applied by us ensures that the left-hand side limiting values of the profiles from the theory agree with the ones from simulations. A comparison of the bulk right-hand side density of B particles ρ_{Br} resulting from the theory and simulations represents a demanding test of the approximations applied.

In Figure 1 we present the results obtained for the system I, i.e., for the size ratio $\sigma_A/\sigma_B = 1$. At low left-hand side bulk densities, (Figure 1a), the fluid seems to be not very structured close to the membrane. The membrane acts as a hard wall for species that cannot penetrate it. This effect combined with the effect of attractive forces between fluid particles and at low left-hand sides bulk density results in the "expulsion" of species A from the region close to membrane plane. The density of species A at the membrane is lower than in the bulk. Similar behavior of the LJ fluids near impermeable walls has been observed and discussed in the literature.[19] The density profile $\rho_B(z)$ on the right-hand side from the membrane exhibits a maximum at the distance close to the membrane, at $z \approx 0.9$. This maximum can be attributed to the presence of species A in the left-hand side "adlayer". The "surface" layer of the particles A on the left-hand side of the membrane acts as an attractive-repulsive wall on the B particles on the right-hand side. The role of repulsive forces seem to be predominant,

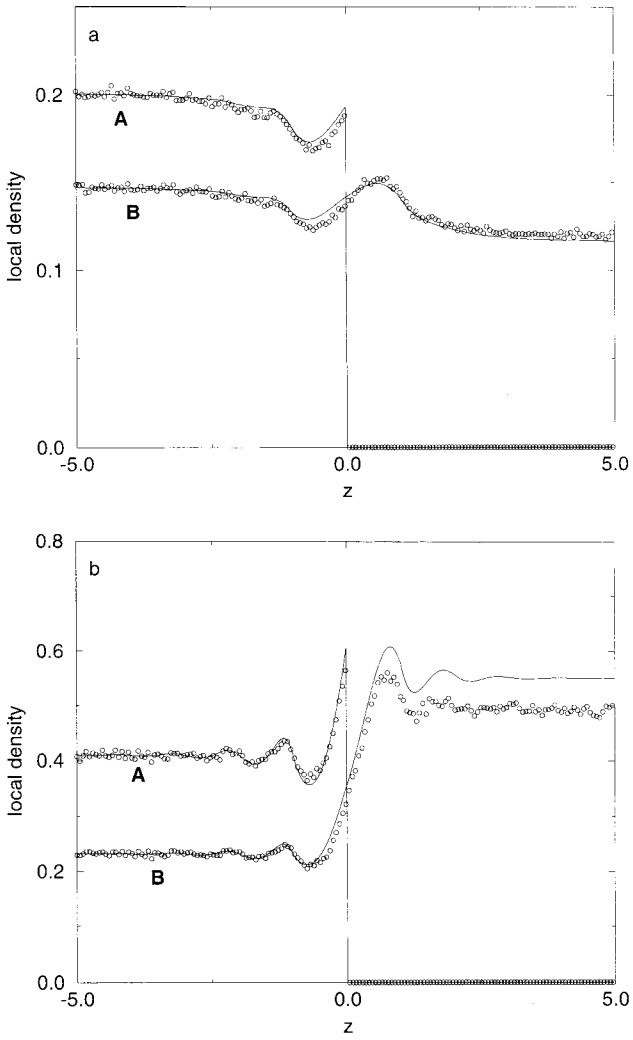

Figure 1. A comparison of the simulated (points) and theoretical (lines) density profiles for the system I at $T^* = 2$. The left-hand side bulk densities are $\rho_{Al} = 0.2007$ and $\rho_{Bl} = 0.1471$ (part a) and $\rho_{Al} = 0.4097$ and $\rho_{Bl} = 0.2324$ (part b). The profiles of particular species are marked by capital letters.

because the position of the maximum almost corresponds to the sum of radii of both species. The agreement between the theoretical and simulation data is good on both sides of the membrane, only small discrepancies in the vicinity of the membrane are observed. It is worth mentioning that the density profiles tend rather slowly to the corresponding bulk values on both sides of the membrane.

In the case of a higher fluid density, Figure 1b (the total left-hand side density is $\rho_{tl} = \rho_{Al}\sigma_{AA}^3 + \rho_{Bl}\sigma_{BB}^3 \approx 0.64$), the left-hand side density profiles exhibit well pronounced layered structure, similar to that observed for hard-sphere system.[8,11] The theoretical predictions are good for $z < 0$ but for $z > 0$ the agreement is less satisfactory. The right-hand side bulk density ρ_{Br} obtained from the density-functional approach is significantly higher than the value obtained form simulation and the entire right-hand side density profile of species B is shifted toward higher values. It means that the theoretical right-hand side pressure p_r is higher than that from simulations. Consequently, the osmotic pressure, $\Pi = p_l - p_r$, where p_l is the left-hand side pressure, would be lower from theory than from simulations. Nevertheless, *T*, the right-hand side theoretical density profile of species B, qualitatively has a similar form to that from simulation.

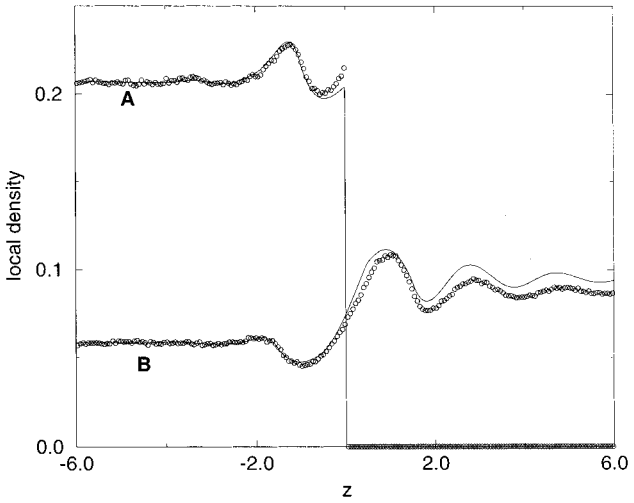

Figure 2. A comparison of the simulated (points) and theoretical (lines) density profiles for the system II at $T^* = 2$. The left-hand side bulk densities are $\rho_{Al} = 0.2069$ and $\rho_{Bl} = 0.0584$. The profiles of particular species are marked by capital letters.

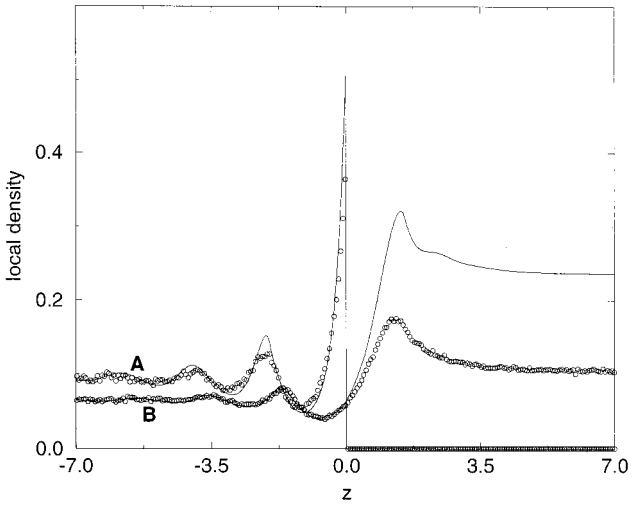

Figure 3. A comparison of the simulated (points) and theoretical (lines) density profiles for the system III at $T^* = 2$. The left-hand side bulk densities are $\rho_{Al} = 0.09459$ and $\rho_{Bl} = 0.0646$. The profiles of particular species are marked by capital letters.

Figure 2 shows the results for the system II, i.e., when $\sigma_A/\sigma_B = 1/2$. The total left-hand side density is $\rho_{tl} = \rho_{Al}\sigma_{AA}^3 + \rho_{Bl}\sigma_{BB}^3 \approx 0.67$. We recall that the size of the smaller component (A in this case) is used here as the unit length. The reduced density of the component B, $\rho_{Bl}\sigma_{BB}^3$ is quite high in this system. The contact value of the nonpermeable species $\rho_A(0^-)$ is lower than the height of the principal maximum of $\rho_A(z)$, due to geometrical constrains resulting from the size ratio. For the same reason the position of the first right-hand side maximum of $\rho_B(z)$ is shifted to about 1.2. The oscillatory character of the density profile $\rho_B(z)$, including phase and magnitude of oscillations, is rather well reproduced by the theory, but the entire profile is slightly shifted to larger values with respect to simulation data.

Finally, in Figure 3 we present results of calculations for the system III. The total left-hand side density is rather high, $\rho_{tl} = 0.82$. The reduced left-hand side bulk density of the nonpermeable component A equals to $\rho_{Al}\sigma_{AA}^3 = 0.7567$. The shape of the density profiles from the density functional theory is similar to that obtained from simulations, however for $z > 0$ a drastic shift in the entire profile $\rho_B(z)$ to higher absolute values is seen. The error in the right-hand side bulk density is large. Also, the agreement of the left-hand side density profiles with simulations is worse than in previous cases.

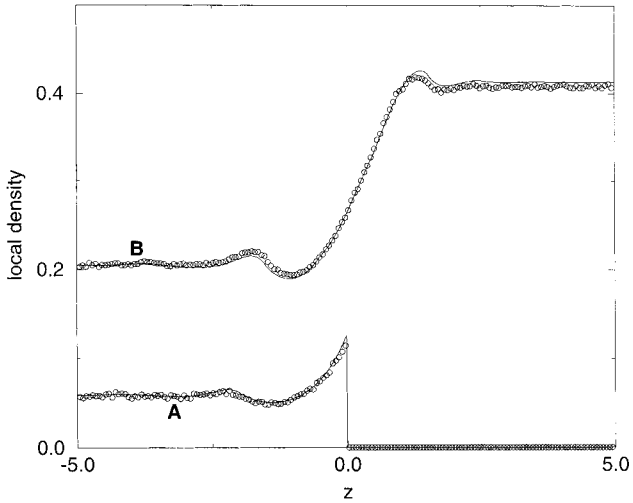

Figure 4. A comparison of the simulated (points) and theoretical (lines) density profiles for the hard sphere system with size ratio $\sigma_{AA}/\sigma_{BB} = 2$. The left-hand side bulk densities are $\rho_{Al} = 0.05959$ and $\rho_{Bl} = 0.2051$. The profiles of particular species are marked by capital letters.

To summarize, the results presented in Figures 1−3 demonstrate that the best agreement of the theory with simulations is obtained when both species are of similar size. When the diameter of particles of permeable component is bigger than that of the nonpermeable one, Figure 2, the agreement is still reasonable. However, theoretical predictions fail when the permeable component is twice smaller than the nonpermeable one and when the total left-hand side density is high. It is worth mentioning that in the case of systems with purely repulsive interparticle forces the agreement of the Kierlik−Rosinberg density functional theory with simulations is quite satisfactory.[11] We have made an additional test by performing calculations for a hard sphere system with the size ratio $\sigma_{AA}/\sigma_{BB} = 2$. Figure 4 shows density profiles resulting from DF theory and canonical Monte Carlo simulations (simulation data are taken from ref 10). The agreement is good. It becomes clear that the inaccuracies for the case of LJ mixtures arise due to an inaccurate treatment of the attractive part of interparticle interactions. In other words, the failing of the DF theory can be attributed to the strict mean field treatment of the LJ interactions. The mean-field approach results in an inaccurate equation of state for the mixture of interest.

Similar difficulties have been encountered in the studies of wetting and drying transitions in the case of a single-component fluid adsorption on a flat solid surface.[2] This problem has been tackled in several ways. For example, Valesco and Tarazona[20] have introduced an additional adjustable parameter into the attractive part of the Lennard-Jones potential. This parameter was chosen to ensure that the bulk coexistence curve obtained from the theory is identical to that obtained from simulation. Another approach was developed by van Swol and Henderson[21] who used modified version of the Tarazona's[2,22] weighted density functional theory. Their method approximates the attractive contribution to the free energy by a polynomial, the coefficients of which have been evaluated fitting the results to simulational data and exact low-density virial results. The Tarazona's weight function[22] has been also modified accordingly. However, application of the above-mentioned approaches to the two-component systems is not instantaneous and would require additional extensive simulational studies.

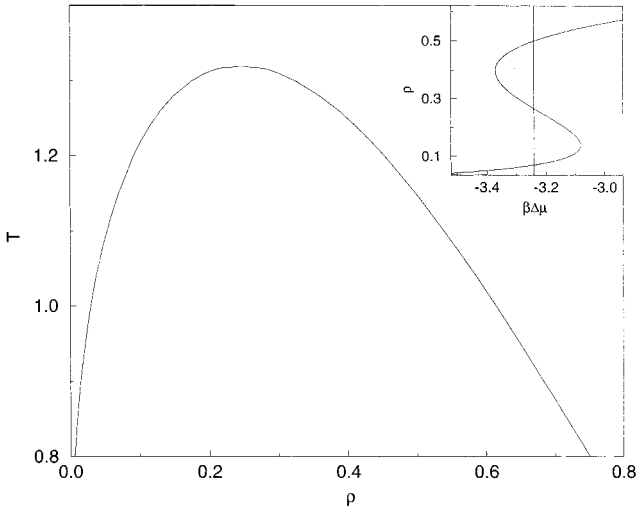

Figure 5. The phase diagram and the dependence of the density on the chemical potential at $T^* = 1.15$ for the Lennard-Jones fluid from the bulk counterpart of the density functional theory.

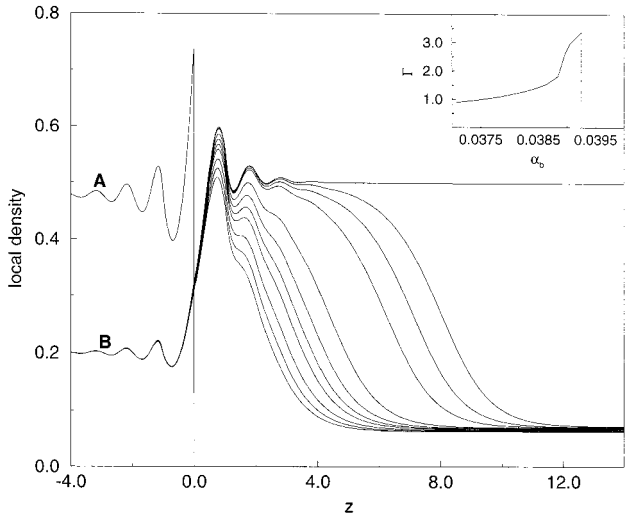

Figure 6. Density profiles for the system I at $T^* = 1.15$. The left-hand side density of the component B is $\rho_{Bl} = 0.2$. The left-hand side densities of the component A are $\rho_{Al} = 0.4775$ (at this density two solutions $\rho_B(z)$ exist), 0.4770, 0.4768, 0.4765, 0.4760, 0.4755, 0.4750, 0.4740, 0.4730, and 0.4720 (the profiles from right to left). For the sake of better visualization only one profile $\rho_A(z)$ (calculated for $\rho_{Al} = 0.4775$) is displayed here. The inset shows the dependence of Γ on α_B. The profiles of particular species are marked by capital letters.

The second series of our calculations has been carried out for the system I at subcritical conditions. It is necessary to mention that in these calculations we have not optimized the effective hard-sphere diameters setting them equal to σ_{ij}.

We would like to begin with a remark that under some conditions the solution of the density functional density profile equation may be nonunique; for some thermodynamic states more than one solution can exist. The bulk systems on both sides of the membrane are Lennard-Jones fluids, and their phase behavior is known. Figure 5 recalls the phase diagram for the considered Lennard-Jones system; the critical temperature is equal to $T^* = 1.315$. The inset shows the dependence of density on the configurational chemical potential at $T^* = 1.15$; the vertical line serves to localize the gas−liquid transition point.

If the two-component system on the left-hand side of the membrane is a thermodynamically stable one-phase fluid, and the chemical potential of the permeable component approaches (from both sides, corresponding to gas and liquid bulk phases) the corresponding value of the chemical potential of a pure Lennard-Jones fluid at the transition point, we can observe the existence of two solutions of the density profile equation. One of them is for gaslike, whereas the second one is for the liquid phase in the bulk part of the system on the right-hand-side of the membrane.

In Figure 6 we show a set of density profiles. The left-hand side bulk density of the permeable component is fixed and equals 0.2, whereas the left-hand side bulk density of the nonpermeable component is varied in such a manner that the value of the configurational chemical potential of the permeable component approaches (from lower values) the value of the configurational chemical potential at the transition point. The latter equals $\beta\Delta\mu_B = -3.2408$. For increasing values of $\beta\Delta\mu_B$ up to -3.2408 (the increase of the chemical potential $\beta\Delta\mu_B$ is enforced by the increase of ρ_{Al}), the thickness of the film of the component B "adsorbed" at the right-hand side of the membrane continuously increases. At $\beta\Delta\mu_B = -3.2408$ two density profiles $\rho_B(z)$ exist, corresponding to two coexisting (cf. Figure 4) bulk gas and bulk liquid densities ρ_{Br}. Instantaneously, in the vicinity of the membrane the left-hand side local densities of both components remain practically unchanged, when the right-hand side density profile $\rho_B(z)$ changes. Obviously, the osmotic pressure for both cases is identical. To characterize the growth of the film on the right-hand side of the membrane we have calculated the "adsorption isotherm" Γ

$$\Gamma = \int_0^\infty dz[\rho_B(z) - \rho_{Br}] \tag{16}$$

The dependence of Γ on activity of B species, $\alpha_B = \exp[\beta\Delta\mu_B]$, is shown in the inset to Figure 6. We observe that the film grows up with the increase of the chemical potential, and when $\beta\Delta\mu_B$ approaches -3.2408, the film thickness remains finite. This growth is continuous; any discontinuity in the growth of the film thickness should be reflected by a jump in Γ. The vertical line in the inset to Figure 6 is at the value of the chemical potential corresponding to the bulk gas−liquid transition on the right-hand side of the system. The values of Γ for $\beta\Delta\mu_B > -3.2408$ correspond to the "adsorption" from a liquid phase on the right-hand side of the system. They are very small (almost zero on the figure scale).

Figure 7 illustrates the changes in the grand canonical potential Ω. The left part shows the total grand canonical potential per unit volume $\Omega^* = \Omega/VkT$, whereas the right part displays the excess grand canonical potential per unit surface area, $\Omega^*_{ex} = \Omega_{ex}/AkT$, $\Omega_{ex} = \lim_{v_l\to\infty, v_r\to\infty}[\Omega + p_l V_l + p_r V_r]$, where p_l, p_r and V_l, V_r are the pressures and volumes of the fluids on both sides of the membrane. The intersection of the two branches of Ω^* in the left part of Figure 7 shows the locus of the bulk gas−fluid transition on the right-hand side of the membrane. The shape of the excess grand potential on the chemical potential is smooth for $\beta\Delta\mu_B < -3.2408$ and for $\beta\Delta\mu_B > -3.2408$. At $\beta\Delta\mu_B = -3.2408$ Ω^*_{ex} is discontinuous. There is no "surface" phase transition; the only transition is the bulk phase transition on the right-hand side of the system. The situation shown in Figure 6 resembles formation of adsorbed film at a weakly adsorbing surface.[2] Actually, the layer of the both components (and the impenetrable component in particular) at the left-hand side of the membrane is the source of the potential field acting on the particles on the other side of the membrane. Formally, this "effective" potential at the distance z from the membrane may be approximated by

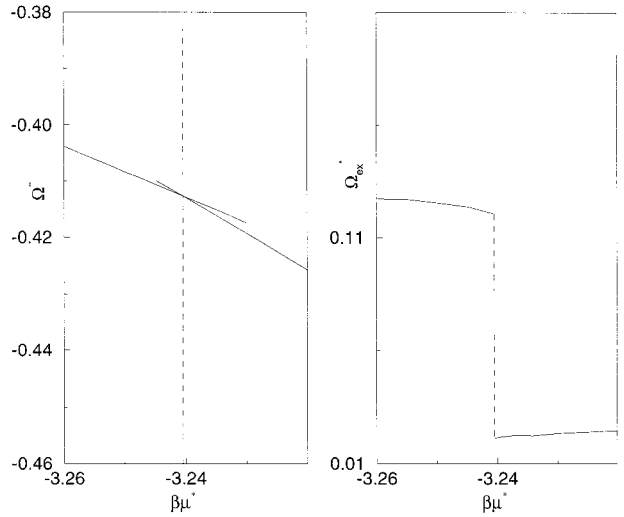

Figure 7. The grand canonical potential per unit volume, Ω* (left panel) and the excess grand canonical potential, Ω^*_{ex} (right panel) for the system I at $T^* = 1.15$. The left-hand side bulk density of the component B is $\rho_{Bl} = 0.2$.

$$v_{eff}(z) = 2\pi\int_{-\infty}^{0} dz'[\rho_A(z')\int_0^{\infty} Ru_{AB}(\sqrt{R^2 + (z - z')^2})dR + \rho_B(z')\int_0^{\infty} Ru_{BB}(\sqrt{R^2 + (z - z')^2})dR] \quad (17)$$

The potential $v_{eff}(z)$ depends on the state condition of the system (i.e., on ρ_{Al} and on ρ_{Bl}). An example of $v_{eff}(z)$, calculated for the system given in Figure 6 at $\beta\Delta\mu_B = -3.2408$ is shown in Figure 8. In comparison with the adsorbing potential for a typical system exhibiting first-order prewetting transition, namely, with the Lennard-Jones (9,3) potential for argon adsorbed on solid carbon dioxide surface,[23] the depth of $v_{eff}(z)$ is approximately 1.5 times shallower and $v_{eff}(z)$ is of shorter range.

Actually, the field $v_{eff}(z)$ created by the surface layer on the left-hand side of the membrane seems to be too weak and its range seems to be insufficient to provide the possibility of the surface phase transition on the right-side of the system. Indeed, performing our calculations for the system I at different temperatures and compositions, we have not encountered a situation which would correspond to a prewetting jump, observed in the case of gas adsorption on a weak substrate.[23] In Figure 9 we show again the density profile for the system I at $T^* = 1.15$. Now, in contrast to the situation displayed in Figure 6, the left-hand side bulk density of the permeable component *B* is lower than the bulk density of the component *A*. At $\beta\Delta\mu_B$ that corresponds to the coexistence point ($\beta\Delta\mu_B = 3.2408$), two solutions for $\rho_B(z)$ exist. The field generated by the layer of A and B particles located at the left-hand side of the membrane is now slightly weaker than in the case of the system displayed in Figure 6, cf. Figure 8. Consequently, the thickness of the film adjacent to the right-hand side of the membrane is smaller. Similarly as previously, the film growth is continuous.

In this work we have applied the density functional approach to evaluate the structure of a two-component Lennard-Jones fluid in contact with a selectively permeable membrane. Our calculations have indicated that the range of applicability of the considered version of the density functional theory is limited to fluids with almost similar diameters of particles belonging to different components. To improve the agreement of the theory with simulations, it would be necessary to propose some modifications of the density functional theory in order to make it capable to reproduce bulk equation of state of one- and two-component systems. One of the possible theoretical routes is to follow the modifications introduced for single-component fluids.[20,21] We have shown that at low temperatures the structure of the permeable fluid component B close to the membrane resembles the structure of a single-component adlayer at a weakly adsorbing solid surface. To characterize this adlayer we have calculated the "adsorption isotherm" Γ. As we have mentioned above, our calculations have not discovered discontinuities on the curve Γ vs $\beta\Delta\mu_B$, connected with the surface phase transitions. A more complex phase behavior of the system may be expected when the interaction energy between distinct species deviates from the Lorentz−Bethelott mixing rule, as well as for the case of more sophisticated membrane-fluid interactions. It seems interesting to include specific interactions between fluid particles and a membrane and to investigate their influence on partitioning of fluid mixtures through selectively permeable membranes as well. We are looking forward to apply the presented theoretical developments to selectively permeable membranes of finite thickness in future studies.

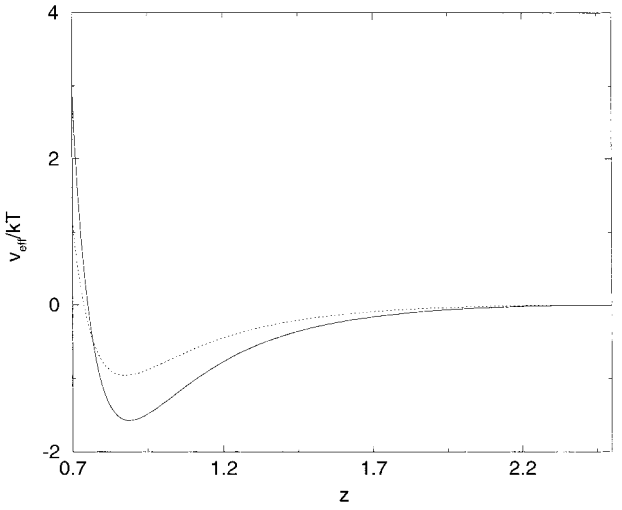

Figure 8. The effective potential $v_{eff}(z)$ for the system I at $T^* = 1.15$, $\rho_{Bl} = 0.2$ and $\rho_{Al} = 0.4775$ (solid line) and for $\rho_{Bl} = 0.385$ and $\rho_{Al} = 0.207$ (dashed line).

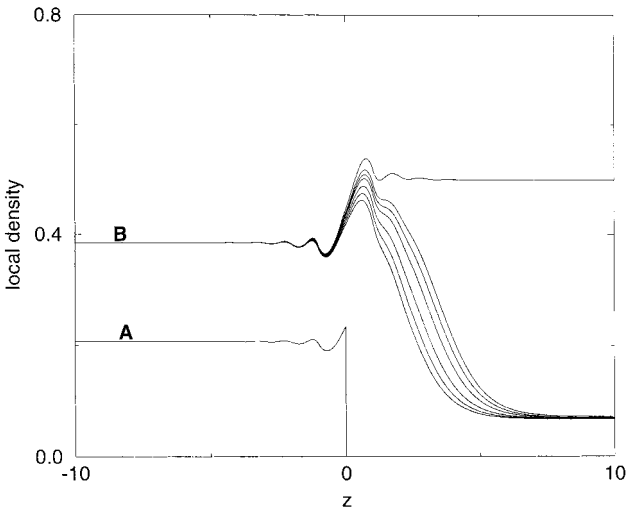

Figure 9. Density profiles for the system I at $T^* = 1.15$. The left-hand side density of the component B is $\rho_{Bl} = 0.385$. The left-hand side densities of the component A are $\rho_{Al} = 0.207$ (at this density two solutions $\rho_B(z)$ exist), 0.2065, 0.206, 0.2055, 0.205, and 0.2045 (the profiles from right to left). For the sake of better visualization only one profile $\rho_A(z)$ (calculated for $\rho_{Al} = 0.207$) is displayed here. The profiles of particular species are marked by capital letters.

Acknowledgment. P.B. thanks KBN for financial support of this work under Grant 3T09A02714. S.S. thanks NATO for financial support under Grant HTECH.CRG972915. O.P. has been supported by DGAPA of the UNAM under Grant IN111597 and CONACyT of Mexico under Grant 25301E. We are grateful to Prof. V. Renugopalakrishnan for critical reading of the manuscript and helpful comments.

References and Notes

(1) Henderson, D. In *Fundamentals of Inhomogeneous Fluids*; Henderson, D., Ed.; M. Dekker: New York, 1992; Chapter 4.
(2) Evans, R. In *Fundamentals of Inhomogeneous Fluids*; Henderson, D., Ed.; M. Dekker: New York, 1992; Chapter 3.
(3) Kroll, D.; Laird, B. *Phys. Rev. A* **1990**, *44*, 4806.
(4) Johnson, K.; Zollneg, J. A.; Gubbins, K. E. *Mol. Phys.* **1993**, *78*, 591.
(5) Marsh, P.; Rickayzen, G.; Calleja, M. *Mol. Phys.* **1995**, *84*, 799.
(6) Margaritis, N.; Rickayzen, G. *Mol. Phys.* **1997**, *90*, 189.
(7) Henderson, D.; Trokhymchuk, A.; Pizio, O. *Chem. Phys. Lett.* **1995**, *245*, 615.
(8) Zhou, Y.; Stell, G. *J. Chem. Phys.* **1988**, *89*, 7010.
(9) Zhou, Y.; Stell, G. *J. Chem. Phys.* **1988**, *89*, 7020.
(10) Bryk, P.; Henderson, D.; Sokołowski, S. *J. Chem. Phys.* **1997**, *107*, 3333.
(11) Bryk, P.; Cyrankiewicz, W.; Borowko, M.; Sokołowski, S. *Mol. Phys.* **1998**, *93*, 111.
(12) Kierlik, E.; Rosinberg, M. L. *Phys. Rev. A* **1990**, *42*, 3382.
(13) Rosenfeld, Y. *Phys. Rev. Lett.* **1989**, *53*, 1989.
(14) Weeks, J. D.; Chandler, D.; Andersen, H. C. *J. Chem. Phys.* **1971**, *54*, 5237.
(15) Barker, A.; Henderson, D. *J. Chem. Phys.* **1967**, *47*, 4714.
(16) Bryk, P.; Patrykiejew, A.; Pizio, O.; Sokołowski, S. *Mol. Phys.* **1997**, *90*, 483.
(17) Bryk, P.; Patrykiejew, A.; Pizio, O.; Sokołowski, S. *Mol. Phys.* **1997**, *92*, 949.
(18) Cracknell, R. F.; Nicholson, D.; Quirke, N. *Mol. Phys.* **1993**, *80*, 885.
(19) Pandit, R.; Schick, M.; Wortis, M. *Phys. Rev. B* **1982**, *26*, 5112.
(20) Valesco, E.; Tarazona, P. *Phys. Rev. A* **1990**, *42*, 2454.
(21) van Swol, F.; and Henderson, J. R. *Phys. Rev. A* **1991**, *43*, 2932.
(22) Tarazona, P. *Phys. Rev. A* **1985**, *31*, 2672.
(23) Sokołowski, S.; Fischer, J. *Phys. Rev. A* **1990**, *41*, 6866.